Cenozoic Pb–Zn–Ag mineralization in the Western Alps

maxime bertauts, Adrien Vezinet, Emilie Janots, Magali Rossi, Isabelle Duhamel-Achin, Philippe Lach, Pierre Lanari

Cenozoic Pb–Zn–Ag mineralization in the Western Alps

Maxime Bertauts[1], Adrien Vezinet[1], Emilie Janots[1], Magali Rossi[2], Isabelle Duhamel-Achin[3], Philippe Lach[4] and Pierre Lanari[5]

[1]*Univ. Grenoble Alpes, Univ. Savoie Mont Blanc, CNRS, IRD, Univ. Gustave Eiffel, ISTerre, 38000 Grenoble, France*

[2]*Univ. Grenoble Alpes, Univ. Savoie Mont-Blanc, CNRS, EDYTEM, 73000 Chambéry, France*

[3]*BRGM, F-13276 Marseille, France*

[4]*BRGM, F-45060 Orléans, France*

[5]*Institut für Geologie, Universität Bern, 3012 Bern, Switzerland*

ABSTRACT

Metallogenic models of polyphase mountain belts critically rely on robust geochronology. We combine petrology with Rb–Sr and U–Th–Pb in situ geochronology, paired at thin-section scale, to date mineralization in deformed hydrothermal Pb–Zn–Ag deposits along an east-west transect in the Western Alps, France. The Pb–Zn–Ag veins occur in shear zones with kinematic structures consistent with the mylonitized host rocks. The ore consists mainly of galena in a quartz-phengite gangue. The paragenesis can be related to hydrothermal crystallization during periods of variable strain. Both isotope systems yield only Cenozoic ages (ca. 35 Ma and 15–20 Ma) without any pre-Alpine inheritance, clearly indicating orogenic mineralization. The metallogenic model proposed here includes significant fluid circulation along major tectonic contacts between basement and sedimentary cover during Alpine convergence.

INTRODUCTION

World-class Pb–Zn–Ag deposits are commonly associated with fluid circulation at basement/cover unconformities in extensive basins (Boiron et al., 2010). However, less-common Pb–Zn–Ag deposits may have an extended evolution influenced by orogenic processes (Williams, 1998) that redistributed the ore minerals (Cugerone et al., 2021). Extracting the ages of crystallization and subsequent remobilization of polymetallic ore deposits has proven challenging due to potential reopening of the isotopic systems (Chiaradia, 2023). Dating actinide-rich accessory minerals is the most common and reliable method for obtaining accurate ages because of the possibility to check for concordance using the triple U–Th–Pb decay series (Rasmussen et al., 2006; Li et al., 2019). However, that approach has limitations due to the relative scarcity and small size of accessory minerals suitable for dating (Engi, 2017). The recent development of in situ Rb–Sr dating (Zack and Hogmalm, 2016) on ubiquitous and abundant minerals (e.g., mica, feldspar, apatite) has opened new avenues for constraining the age of deposits as young as 28.1 ± 2.2 Ma (Şengün et al., 2019). The Rb–Sr method can assess not only the primary age but also subsequent periods of mineralization (Olierook et al., 2020; Tillberg et al., 2021). Proterozoic Rb–Sr ages preserved within Caledonian ore bodies imply inheritance and remobilization during the subsequent orogenic stages (Tillberg et al., 2021).

Our study investigates the timing and tempo of Pb–Zn–Ag mineralization along a lithostructural profile in the Western Alps in France, where the tectonic and metamorphic evolution and fluid circulation are well constrained (Handy et al., 2010; Gnos et al., 2021). The abundance of Pb–Zn–Ag mineralization in this area has been attributed to Variscan orogenesis, Mesozoic Tethyan opening, or Alpine remobilization (Nägler et al., 1995). However, recent in situ U–Pb dating by Bertauts et al. (2022) of stratabound Pb–Zn–Ag deposits at Mâcot-la Plagne and

Peisey-Nancroix (southeastern France) suggests a new Alpine orogenic period of metallization. To consolidate these results, we used a multi-system approach involving in situ U–Th–Pb and Rb–Sr dating to compare and constrain ages.

GEOLOGY AND SAMPLING

Samples were collected along an east-west transect from the Briançonnais domain of the internal Alps to the Belledonne external crystalline massif (Fig. 1). The Briançonnais domain corresponds to the European continental margin and consists of Variscan basement comprising Carboniferous schists and locally some Mesozoic sediments. It was partially subducted under the African tectonic plate before being thrust over the European tectonic plate during the Cenozoic Alpine convergence (Handy et al., 2010). The sedimentary cover is characterized by low-temperature metamorphism (<500 °C) and intense deformation (Strzerzynski et al., 2012). The Belledonne massif is composed of Variscan basement rocks of the European plate, which underwent lower greenschist facies metamorphism and only localized deformation during the Alpine collision (Rossi et al., 2005). The internal metamorphic Alps are separated from the external Alps by the Penninic front, which marks the onset of the European margin collision at ca. 35 Ma (Ceriani et al., 2001).

We collected 44 samples from mine tailings of seven historic Pb–Zn–Ag deposits. Of these, only four samples from two different lithostructural contexts contain accessory allanite and monazite suitable for U–Th–Pb dating. In the internal Briançonnais domain, one sample from the Peisey-Nancroix deposit is located within the deformed Permian–Triassic cover along the Internal Briançonnais fault (IBF; Fig. 1). In the Belledonne massif, the three samples come from the subsidiary Pb–Zn–Ag mineralization of the Penay and Le Gros Villan deposits, which are located in sub-vertical northeast-southwest dextral shear zones along major faults separating the massif from the Mesozoic cover (Fig. 1).

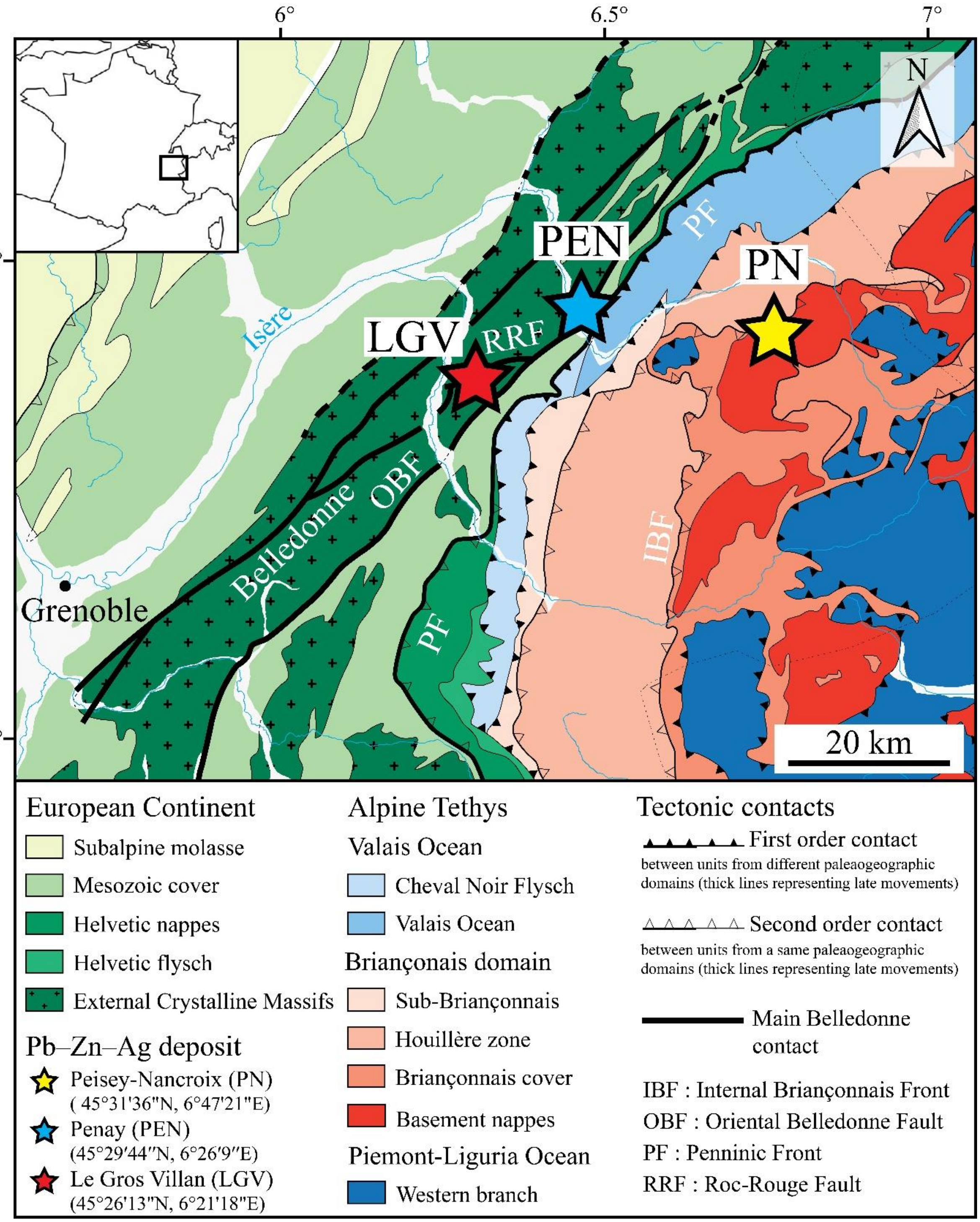

Figure 1. Location of the studied Pb–Zn–Ag mineralizations on the tectonic map of the Western Alps (northern French Alps), modified from Bousquet et al. (2012).

RESULTS

Mineralogy and Microstructures

The Pb–Zn–Ag mineralization consists mainly of galena with variable amounts of chalcopyrite, sphalerite, tetrahedrite-tennantite, and pyrite. The four samples show evidence of a high-strain regime with clasts hosted in a fine-grained equigranular recrystallized matrix.

Based on mineralogy and microstructures (Bertauts et al., 2022), mineralization in the Peisey-Nancroix deposit appears to be synchronous with dynamic quartz recrystallization associated with the precipitation of phengite (Fig. 2A) and monazite (Fig. 2B). The Penay sample shows massive sphalerite in a galena-sphalerite matrix. Clasts of albite, quartz, and foliated phengite aggregates are found within the massive sphalerite and recrystallized matrix (Fig. 2C). Subhedral to anhedral allanite grains are intergrown with sulfides (galena and sphalerite) and phengite contains inclusions of these minerals, indicating a common origin (Fig. 2D). The Le Gros Villan mineralization consists of centimeter-long galena-chalcopyrite-sphalerite-quartz veins hosted in a matrix of recrystallized, partially sericitized quartz and K-feldspar clasts. Phengite that formed at this stage is referred to herein as Ph1. Fractures within the K-feldspar clasts are filled by sulfides (galena and chalcopyrite). Monazite occurs as inclusions within other minerals and forms part of intergrowths with sulfides (Fig. 2F). Hourglass sector zoning within the monazite indicates a single crystallization stage during primary mineralization. The primary mineralization is affected by a second stage of deformation and recrystallization expressed by a foliation made of phengite (Ph2) and secondary fine-grained foliated galena (Gn2) that in places cuts the primary sulfides (Fig. 2E). In these foliated domains, the shape of monazite grains is controlled by foliation deflection of oriented acicular phengite grains.

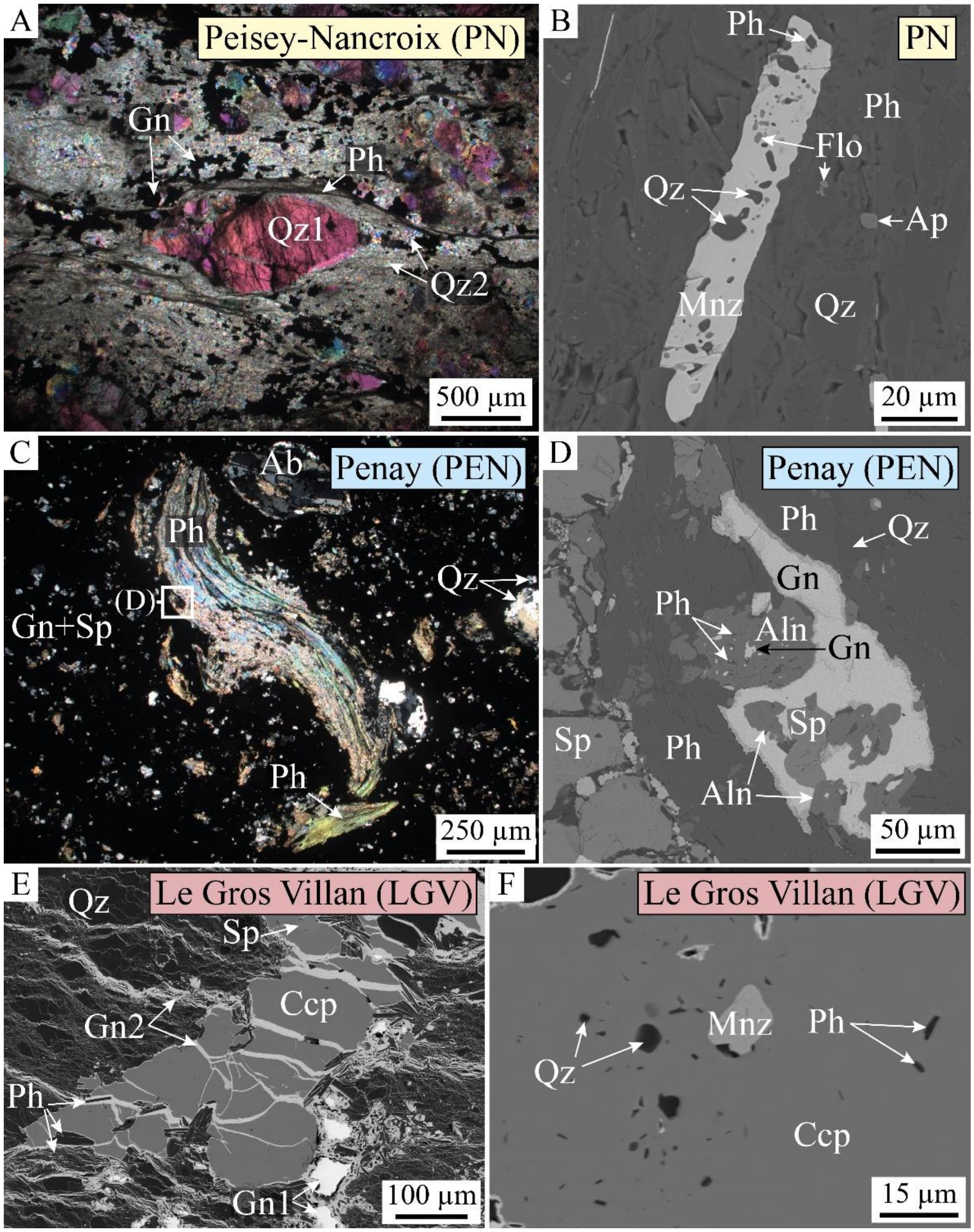

Figure 2. Examples of analyzed phengite (A, C, E) and accessory minerals (B, D, F) used for dating, observed using optical (A, C) and backscattered electron (B, D, E, F) microscopy. The two Peisey-Nancroix samples show: (A) deformed quartz (Qz) Qz1 porphyroclasts shaped by micrometric phengite (Ph) oriented in the foliation, sulfides, and equigranular micrograins of Qz2 (thick section, polarized light) (Gn—galena); and (B) prismatic monazite (Mnz) grain with a poikilitic texture highlighted by quartz, spherical florencite (Flo), and acicular phengite inclusions (Ap—apatite). The massive sulfides from thin sections of Penay show: (C) porphyroclasts of a foliated phengite foliated and folded, albite (Ab), and quartz hosted in a sphalerite-galena matrix (Gn + Sp); and (D) intergrowth texture between galena, sphalerite, and anhedral allanite (Aln) grains within the foliated phengite clast. The sample from Le Gros Villan shows: (E) chalcopyrite (Ccp) cracks filled by oriented acicular phengite and Gn2 crystallization; and (F) subhedral monazite inclusion within chalcopyrite. Abbreviations from Warr (2021).

Electron microprobe point analysis and X-ray mapping demonstrated that phengite from the three deposits have homogeneous major and minor element compositions (Tab1e S1 and Figs. S1 and S2 in the Supplemental Material1).

In situ LA-ICP-MS Rb–Sr and U–Th–Pb Dating

The U–Pb analyses on 26 monazite grains from the Peisey-Nancroix deposit (Fig. 3A; Table S5) define an isochron in the Tera-Wasserburg diagram that intersects the Concordia at 35.1 ± 0.6 Ma (Bertauts et al., 2022). This age is similar to that obtained on 52 in situ Rb–Sr isotopic analyses on five phengite crystal aggregates (Table S8) showing 87Rb/86Sr values ranging from 350 to 800, aligned along an array with a slope corresponding to an age of 34.6 ± 4.7 Ma with an initial 87Sr/86Sr value of 0.771 ± 0.034. Two spots have higher Sr contents and Rb/Sr values <70, which could correspond to phengite with higher Sr contents or inclusions of Sr-rich minerals such as apatite. When these two spots are added, the resulting isochron gives an older age of 40.1 ± 3.2 Ma with an initial Sr isotope ratio of 0.724 ± 0.014 (Fig. 3B).

The Th–Pb analyses of allanite from the Penay deposit (Table S7) are plotted in an isochron diagram 208Pb/206Pbc (c—common) versus 232Th/206Pbc (n = 10, Fig. 3C). The regression yields a Th/Pb age for allanite of 14.9 ± 7.6 Ma. In situ Rb–Sr isotope analyses of three Penay phengite aggregates located within massive sphalerite or fine-grained galena-sphalerite matrix (Table S8) define an isochron age of 18.4 ± 7.2 Ma (n = 35) with an initial 87Sr/86Sr value of 0.7214 ± 0.0065 consistent with the Th–Pb age. Six analyses of co-genetic albite grains yield a scattered Sr-isotope weighted mean of 0.7213 ± 0.0030. When included in the regression, the age remains the same, but the uncertainty of the isochron regression decreases to 3.6 Ma (Fig. 3D).

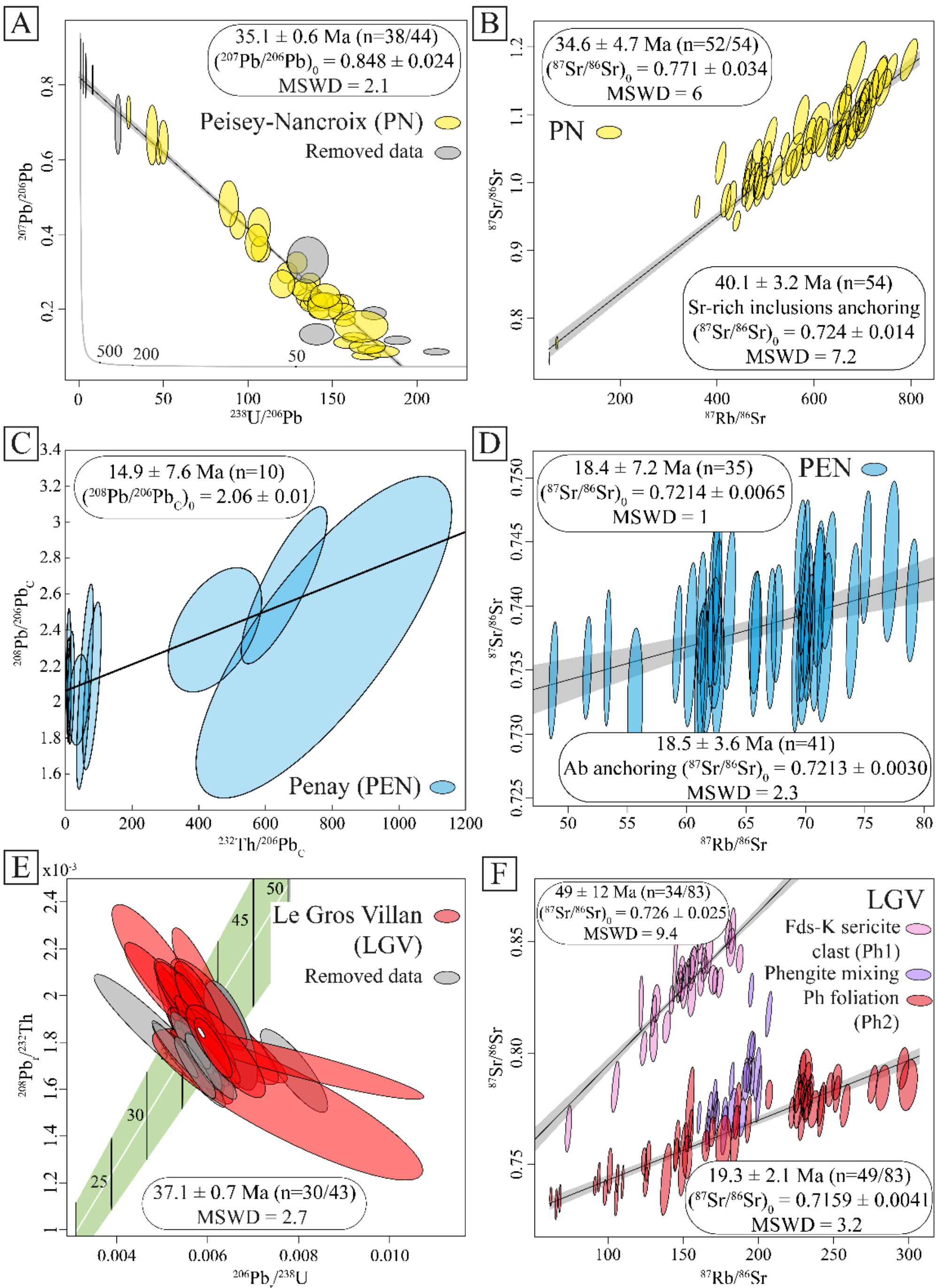

Figure 3. U–Pb (A, C, E) and Rb–Sr (B, D, F) laser ablation–inductively coupled plasma–mass spectrometry analyses on rare earth element–rich phases and phengite (Ph), respectively, for the Peisey-Nancroix (PN) (A, B), Penay (PEN) (C, D) and Le Gros Villan (LGV) (E, F) mineralizations. (A) Tera-Wasserburg diagram of PN monazite without any correction from Bertauts et al. (2022). (C) 206Pbc normalized Th–Pb isochron of PEN allanite. (E) U–Th–Pb data from LGV monazite are plotted on a 208Pbr/232Th versus 206Pbr/238U Concordia diagram using the total Pb/U–Th algorithm of Vermeesch (2020). Rb–Sr isochrons and calculated ages for (B) PN sample; (D) PEN sample (Ab—albite); and (F) LGV sample. Fds-K—K-feldspar. Data ellipses represent 2σ errors. MSWD—mean square of weighted deviates.

The U–Th–Pb monazite dating from the Le Gros Villan deposit was performed on 22 monazite grains obtained from two different thin sections (Table S6). After common Pb correction for the three Pb isotopes (206Pb, 207Pb, and 208Pb), the monazite data yield a Concordia age of 37.1 ± 0.7 Ma (n = 30/43) on a 208Pbr/232Th (r—radiogenic) versus 206Pbr/238U diagram (Fig. 3E). Furthermore, Rb–Sr isotopic analyses were also performed on 10 phengite clusters (Table S8) within sericitized feldspar (Ph1) or secondary foliation (Ph2). All data from the Ph2 foliation align along an isochron that yields an age of 19.3 ± 2.1 Ma. In comparison, the Ph1 results are more complex to interpret, but phengites in one clast plot on a Rb–Sr linear array give an age of 49 ± 12 Ma, overlapping the U–Th–Pb age. The other analyses plot between the two isochrons between ca. 49 and 19 Ma (Fig. 3F).

DISCUSSION

Strenght of U–Th–Pb and Rb–Sr Geochronology

In fluid-rich environments, the Rb–Sr isochron ages are generally recording the phengite crystallization age (Glodny et al., 2008; Villa, 2016). To prepare the groundwork for in situ dating, careful mineralogical and microstructural relationships were established to determine the crystallization sequences. Homogeneous major and minor elements compositions of phengite are interpreted as one phengite population without recrystallizations (Fig. S1 and Fig. S2). Intergrowth and inclusion relationships (Fig. 2), as well as mineral zoning, indicate that the phengite and REE-minerals are cogenetic. Except Ph2 from the Le Gros-Villan, they coincide with the main stage of sulfide precipitation and thus record the primary age of the Pb–Zn–Ag deposits. Indeed, there is equilibration of the two isotopic systems (Rb–Sr and U–Th–Pb) giving consistent Alpine ages (Fig. 3). Even in the more complex case of the Le Gros Villan deposit, the primary phengite (Ph1) which corresponds to sericitization of K-feldspar, has scattered Rb–Sr isotopic analyses but with a discrete alignment at 49 ± 12 Ma. This older age overlaps with the U–Th–Pb age of the monazite (37.1 ± 0.7 Ma) attributed to the primary mineralization (Fig. 2E, F), with probably some inheritance from K-feldspar. Such results clearly demonstrate the strength of the in situ method used here, because mixing between incompletely reset mica and/or K-feldspar domains has been a recurring problem in solution-based studies (e.g., Müller et al., 1999; Bröcker et al., 2013).

The U–Th–Pb dating was complicated by two factors: (i) the scarcity and small size of mineral grains suitable for dating, with only 3 samples out of 44 yielding suitable material, and (2) the possible incorporation of common Pb in this Pb-rich environment, as seen for the Le Gros Villan monazite and, more importantly, for the Penay allanite. In contrast, the ubiquity of mica, the structural control of this mineral, and minimal sample preparation, are advantages of the Rb–Sr system when used for dating of orogenic mineralization. With a wide range of Rb/Sr ratios, in situ dating of white mica can yield a well-resolved Alpine age of 19.3 Ma ± 2.1 Ma for the Le Gros Villan deposit without isochron anchoring by other phases (10% precision). For samples with lower Rb/Sr spreading (40% precision), isochron anchoring with co-genetic Sr-rich phases improves the precision by about 20%. For samples from the Peisey-Nancroix deposit, isochron anchoring modifies the initial $^{87}Sr/^{86}Sr$ value and thus the calculated age, but within the range of uncertainties (40.1 Ma ± 3.2 Ma instead of 34.6 ± 4.7 Ma). The Rb/Sr calibration on the Mica-Mg nano-powder (Tab. S9) may induce a few percent drifted phengite age, but this would represent less than 1 Ma for such young deposit within the uncertainty.

Another advantage of cross-comparison of Rb–Sr and U–Th–Pb dating paired in thin section is the ability to distinguish different crystallization stages (Chiaradia, 2023). The primary Eocene mineralization of the Le Gros Villan deposit (37.1 ± 0.7 Ma, monazite) contains secondary phengite (Ph2) and galena (Gn2) in post-mineralization microstructures (localized foliation and fractures, Fig. 2E). Thus, Ph2 in this deposit is thought to record secondary Miocene remobilization at 19.3 ± 2.1 Ma during deformation. In this case, two Rb–Sr ages correspond to two distinct microstructures (Fig. 3).

Evidence of Alpine Mineralization and Remobilization

In Peisey-Nancroix, one of the two largest historical Pb–Zn–Ag deposits from the French Alps, the new Rb–Sr dating (Fig. 3B) is consistent with the well-resolved U–Pb syn-orogenic Alpine ages from Bertauts et al. (2022), ruling out a possible sedimentary-diagenetic origin or inheritance for these deposits despite their presence in Triassic quartzite (Rogel, 1961). The deposits formed over a short period of time, which was less than the analytical resolution of in situ U–Pb dating (35.1 ± 0.6 Ma) and Rb–Sr dating (35–40 Ma). The age of ca. 35 Ma is attributed to fluid circulation coeval with the major top-to-west thrusting within the Penninic front (and the Internal Briançonnais front) at the onset of the collision (Strzerzynski et al., 2012).

The two deposits in the external crystalline massifs are located in the Variscan basement and show evidence of sulfide recrystallization, suggesting episodic growth and/or remobilization. However, neither in situ U–Th–Pb dating of REE-rich phases nor Rb–Sr dating of white mica indicate a pre-Alpine age. The Miocene ages (15–20 Ma) obtained in these deposits could correspond to the circulation of non-mineralizing fluids (Rolland and Rossi, 2016). The new Late Eocene U–Th–Pb monazite ages in the Le Gros Villan mineralization (Fig. 3E) document early, previously undocumented fluid circulation and are more comparable to those obtained in the internal domains (Gnos et al., 2021). In the external domains, sedimentation had started in a flexural basin, and thrusting in the internal domain along the Penninic front had just begun (Simon-

Labric et al., 2009). Thus, early mineralization in the Belledonne massif basement may have been promoted by fluid circulation in Variscan-inherited structures reactivated during burial of the massif (Guillot and Ménot, 2009).

CONCLUSIONS

Concordance of the paired in situ Rb–Sr and U–Th–Pb ages in the Western Alps suggests that these isotopic systems reached equilibrium during hydrothermal Pb–Zn–Ag mineralization. The combination of Rb–Sr and U–Th–Pb systems unambiguously indicates Alpine ages for these Pb–Zn–Ag deposits. Two ages, 35–40 Ma and 15–20 Ma, are associated with collision and exhumation of the Belledonne massif. The Rb–Sr geochronological data set obtained on texturally distinctive micas provides evidence for episodic evolution of Alpine Pb–Zn–Ag mineralization. The Pb–Zn–Ag mineralization was produced by fluid circulation along major lithostructural contacts during the Alpine collision.

ACKNOWLEDGMENTS

This work was initially supported by the "Référentiel Géologique de la France" RGF-Alps Program of the Bureau de Recherche Géologiques et Minières (BRGM), which financed the Ph.D. grant of M. Bertauts. Additional support was received from the TelluS Program of Centre National de la Recherche Scientifique / Institut national des sciences de l'Univers (CNRS/INSU), the IDEX-Initiative de Recherche à Grenoble Alpes 2021 funding provided by the University Grenoble Alpes, and local BQR funding. The work was mainly carried out at l'Institut des Sciences de la Terre (ISTerre, Université Grenoble Alpes), which is part of the Laboratoires d'excellence (LabEx) OSUG@2020 (ANR10 LABX56). Rb–Sr analyses were conducted in the ISTerre

MicroAnalytical Platform (IMAP) at Université Grenoble Alpes, funded by grants from the European Research Council (ERC) under the European Union's Horizon H2020 research and innovation program (Synergy Grant MEET, grant agreement no. 856555); Auvergne-Rhône-Alpes region (2020 AURA P3 – CPER 2015/2020) and CNRS-INSU. We acknowledge the support of the French Agence Nationale de la Recherche (ANR), under grant ANR-23-CE01-0017 (project CMiO). The three anonymous reviewers helped with clarifying several aspects of the paper and are sincerely acknowledged.

REFERENCES CITED

Bertauts, M., Janots, E., Rossi, M., Duhamel-Achin, I., Boiron, M.-C., Airaghi, L., Lanari, P., Lach, P., Peiffert, C., and Magnin, V., 2022, A New Alpine Metallogenic Model for the Pb-Ag Orogenic Deposits of Macôt-la Plagne and Peisey-Nancroix (Western Alps, France): Geosciences, v. 12, p. 331, https://doi.org/10.3390/geosciences12090331.

Boiron, M.-C., Cathelineau, M., and Richard, A., 2010, Fluid flows and metal deposition near basement /cover unconformity: lessons and analogies from Pb-Zn-F-Ba systems for the understanding of Proterozoic U deposits: Geofluids, v. 10, p. 270–292, https://doi.org/10.1111/j.1468-8123.2010.00289.x.

Bousquet, R., Schmid, S.M., Zeilinger, G., Oberhänsli, R., Rosenberg, C., Molli, G., Robert, C., Wiederkehr, M., and Rossi, P., 2012, Tectonic framework of the Alps: Commission for the geological map of the world (www.geodynalps.org).

Bröcker, M., Baldwin, S., and Arkudas, R., 2013, The geological significance of 40Ar/ 39Ar and Rb-Sr white mica ages from Syros and Sifnos, Greece: a record of continuous (re)crystallization during exhumation? Journal of Metamorphic Geology, v. 31, p. 629–646, https://doi.org/10.1111/jmg.12037.

Ceriani, S., Fügenschuh, B., and Schmid, S.M., 2001, Multi-stage thrusting at the “Penninic Front” in the Western Alps between Mont Blanc and Pelvoux massifs: International Journal of Earth Sciences, v. 90, p. 685–702, https://doi.org/10.1007/s005310000188.

Chiaradia, M., 2023, Radiometric Dating Applied to Ore Deposits: Theory and Methods, *in* Huston, D. and Gutzmer, J. eds., Isotopes in Economic Geology, Metallogenesis and Exploration, Cham, Springer International Publishing, Mineral Resource Reviews, p. 15–35, https://doi.org/10.1007/978-3-031-27897-6_2.

Cugerone, A., Cenki-Tok, B., Muñoz, M., Kouzmanov, K., Oliot, E., Motto-Ros, V., and Le Goff, E., 2021, Behavior of critical metals in metamorphosed Pb-Zn ore deposits: example from the Pyrenean Axial Zone: Mineralium Deposita, v. 56, p. 685–705, https://doi.org/10.1007/s00126-020-01000-9.

Engi, M., 2017, Petrochronology Based on REE-Minerals: Monazite, Allanite, Xenotime, Apatite: Reviews in Mineralogy and Geochemistry, v. 83, p. 365–418, https://doi.org/10.2138/rmg.2017.83.12.

Glodny, J., Kühn, A., and Austrheim, H., 2008, Diffusion versus recrystallization processes in Rb–Sr geochronology: Isotopic relics in eclogite facies rocks, Western Gneiss Region, Norway: Geochimica et Cosmochimica Acta, v. 72, p. 506–525, https://doi.org/10.1016/j.gca.2007.10.021.

Gnos, E., Mullis, J., Ricchi, E., Bergemann, C.A., Janots, E., and Berger, A., 2021, Episodes of fissure formation in the Alps: connecting quartz fluid inclusion, fissure monazite age, and fissure orientation data: Swiss Journal of Geosciences, v. 114, p. 14, https://doi.org/10.1186/s00015-021-00391-9.

Guillot, S., and Ménot, R.-P., 2009, Paleozoic evolution of the External Crystalline Massifs of the Western Alps: Comptes Rendus Geoscience, v. 341, p. 253–265, https://doi.org/10.1016/j.crte.2008.11.010.

Handy, M.R., M. Schmid, S., Bousquet, R., Kissling, E., and Bernoulli, D., 2010, Reconciling plate-tectonic reconstructions of Alpine Tethys with the geological–geophysical record of spreading and subduction in the Alps: Earth-Science Reviews, v. 102, p. 121–158, https://doi.org/10.1016/j.earscirev.2010.06.002.

Li, L.-X., Zi, J.-W., Li, H.-M., Rasmussen, B., Wilde, S.A., Sheppard, S., Ma, Y.-B., Meng, J., and Song, Z., 2019, High-Grade Magnetite Mineralization at 1.86 Ga in Neoarchean Banded Iron Formations, Gongchangling, China: In Situ U-Pb Geochronology of Metamorphic-Hydrothermal Zircon and Monazite: Economic Geology, v. 114, p. 1159–1175, https://doi.org/10.5382/econgeo.4678.

Müller, W., Dallmeyer, R.D., Neubauer, F., and Thöni, M., 1999, Deformation-induced resetting of Rb/Sr and 40Ar/39Ar mineral systems in a low-grade, polymetamorphic terrane (Eastern Alps, Austria): Journal of the Geological Society, v. 156, p. 261–278, https://doi.org/10.1144/gsjgs.156.2.0261.

Nägler, Th.F., Pettke, Th., and Marshall, D., 1995, Initial isotopic heterogeneity and secondary disturbance of the Sm-Nd system in fluorites and fluid inclusions: A study on mesothermal veins from the central and western Swiss Alps: Chemical Geology, v. 125, p. 241–248, https://doi.org/10.1016/0009-2541(95)00091-Y.

Olierook, H.K.H. et al., 2020, Resolving multiple geological events using in situ Rb–Sr geochronology: implications for metallogenesis at Tropicana, Western Australia: Geochronology, v. 2, p. 283–303, https://doi.org/10.5194/gchron-2-283-2020.

Rasmussen, B., Sheppard, S., and Fletcher, I.R., 2006, Testing ore deposit models using in situ U-Pb geochronology of hydrothermal monazite: Paleoproterozoic gold mineralization in northern Australia: Geology, v. 34, p. 77, https://doi.org/10.1130/G22058.1.

Rogel, P., 1961, Le gisement de Plomb de La Plagne (Savoie). Etude géologique et métallogénique [Thèse de 3e cycle]: Faculté des sciences de l’université de Paris, 74 p.

Rolland, Y., and Rossi, M., 2016, Two-stage fluid flow and element transfers in shear zones during collision burial-exhumation cycle: Insights from the Mont Blanc Crystalline Massif (Western Alps): Journal of Geodynamics, v. 101, p. 88–108, https://doi.org/10.1016/j.jog.2016.03.016.

Rossi, M., Rolland, Y., Vidal, O., and Cox, S.F., 2005, Geochemical variations and element transfer during shear-zone development and related episyenites at middle crust depths: insights from the Mont Blanc granite (French — Italian Alps): Geological Society, London, Special Publications, v. 245, p. 373–396, https://doi.org/10.1144/GSL.SP.2005.245.01.18.

Şengün, F., Erlandsson, V.B., Hogmalm, J., and Zack, T., 2019, In situ Rb-Sr dating of K-bearing minerals from the orogenic Akçaabat gold deposit in the Menderes Massif, Western Anatolia, Turkey: Journal of Asian Earth Sciences, v. 185, p. 104048, https://doi.org/10.1016/j.jseaes.2019.104048.

Simon-Labric, T., Rolland, Y., Dumont, T., Heymes, T., Authemayou, C., Corsini, M., and Fornari, M., 2009, 40Ar/39Ar dating of Penninic Front tectonic displacement (W Alps) during the Lower Oligocene (31-34 Ma): Terra Nova, v. 21, p. 127–136, https://doi.org/10.1111/j.1365-3121.2009.00865.x.

Strzerzynski, P., Guillot, S., Leloup, P.H., Arnaud, N., Vidal, O., Ledru, P., Courrioux, G., and Darmendrail, X., 2012, Tectono-metamorphic evolution of the Briançonnais zone (Modane-Aussois and Southern Vanoise units, Lyon Turin transect, Western Alps): Journal of Geodynamics, v. 56–57, p. 55–75, https://doi.org/10.1016/j.jog.2011.11.010.

Tillberg, M., Drake, H., Zack, T., Hogmalm, J., Kooijman, E., and Åström, M., 2021, Reconstructing craton-scale tectonic events via in situ Rb-Sr geochronology of poly-phased vein mineralization: Terra Nova, v. 33, p. 502–510, https://doi.org/10.1111/ter.12542.

Vermeesch, P., 2020, Unifying the U–Pb and Th–Pb methods: joint isochron regression and common Pb correction: Geochronology, v. 2, p. 119–131, https://doi.org/10.5194/gchron-2-119-2020.

Villa, I.M., 2016, Diffusion in mineral geochronometers: Present and absent: Chemical Geology, v. 420, p. 1–10, https://doi.org/10.1016/j.chemgeo.2015.11.001.

Warr, L.N., 2021, IMA–CNMNC approved mineral symbols: Mineralogical Magazine, v. 85, p. 291–320, https://doi.org/10.1180/mgm.2021.43.

Williams, P.J., 1998, Metalliferous economic geology of the Mt Isa Eastern Succession, Queensland: Australian Journal of Earth Sciences, v. 45, p. 329–341, https://doi.org/10.1080/08120099808728395.

Zack, T., and Hogmalm, K.J., 2016, Laser ablation Rb/Sr dating by online chemical separation of Rb and Sr in an oxygen-filled reaction cell: Chemical Geology, v. 437, p. 120–133, https://doi.org/10.1016/j.chemgeo.2016.05.027.

[1]Supplemental Material. Analytical methods and monazite U–Th–Pb, allanite Th–Pb, and phengite Rb–Sr data analysis for the Pb–Zn–Ag deposits in the French Northern Alps; chemical map with summary table of the phengite and albite compositions; Tables S1–S8; and Figures S1 and S2. Please visit https://doi .org /10 .1130 /GEOL .S.25209137 to access the supplemental material; contact editing@geosociety.org with any questions.